www.czasopisma.pan.pl PAN www.journals.pan.pl
Chemical and Process Engineering 2021, 42 (3), 235–252
DOI: 10.24425/cpe.2021.138928

Modelling of methane dry reforming over Ni/CaO–Al_2O_3 catalyst

Robert Cherbański[1], Ewelina Franczyk[2], Michał Lewak[1], Piotr Machniewski[1], Eugeniusz Molga[1*]

[1]Warsaw University of Technology, Faculty of Chemical and Process Engineering, ul. Waryńskiego 1, 00-645 Warsaw, Poland

[2]Łukasiewicz Research Network – New Chemical Syntheses Institute, Al. Tysiąclecia Państwa Polskiego 13a, 24-110 Puławy, Poland

In memory of Professor Jerzy Bałdyga – our colleague, friend and teacher

This paper presents the results of investigations into dry methane reforming (DMR). The process was aimed at obtaining synthesis gas required for the production of dimethyl ether (DME). The effect of temperature, pressure and inlet gas composition on the process was determined in the experimental part of this work. The tests were carried out in a laboratory tubular reactor over a Ni/CaO–Al_2O_3 catalyst. The obtained experimental results were used to verify literature kinetic data and to develop a mathematical model of the DMR process.

Keywords: dry methane reforming, dimethyl ether, nickel catalyst, kinetics, modelling

1. INTRODUCTION

The production of synthesis gas from methane is one of the most important processes in the chemical industry. Syngas is a feedstock used in many chemical syntheses, among others for the production of ammonia, methanol, etc. It is also used as a hydrogen source. Recently, there has been a growing interest in the use of syngas to produce dimethyl ether (DME), which is considered to be the green fuel of the future.

Syngas obtained in DMR process, after removing of water vapour, is a mixture of unconverted methane and carbon dioxide as well as products: hydrogen and carbon monoxide. The contribution of individual compounds depends on the composition of the inlet gas stream, the type of catalyst and the process operating conditions. In industry, syngas is produced using the following methods: steam methane reforming (SMR), dry methane reforming (DMR), catalytic partial oxidation of methane (POM), and autothermal reforming (ATR) (Borowiecki and Gołębiowski, 2005; Collodi and Wheeler, 2010; Enger et al., 2008; Pena et al., 1996; Rostrup-Nielsen et al., 2002; Wender, 1996; York et al., 2003).

* Corresponding author, e-mail: eugeniusz.molga@pw.edu.pl

A synthetic summary of three main methane conversion processes is presented in Table 1. This table shows that DMR is the best method to obtain DME because of the equimolar ratio of hydrogen to carbon monoxide in the produced syngas, and a possible use of carbon dioxide being a by-product in the synthesis of DME. Recycling of the produced CO_2 to the methane reforming unit makes it possible to obtain the synthesis gas with the desired composition. Also, it improves the ecological aspects of DME production by reducing CO_2 emissions.

Table 1. Methods of methane reforming processes – basic characteristics

	Method		
Parameters	Dry Methane Reforming (DMR)	Steam Methane Reforming (SMR)	Partial Oxidation of Methane (POM)
Main reaction	$CH_4+CO_2 \rightarrow 2CO+2H_2$	$CH_4+H_2O \rightarrow CO+3H_2$	$2CH_4+O_2 \rightarrow 2CO+4H_2$
Molar ratio of CH_4/X at the reactor inlet $X = CO_2, H_2O, O_2$	1 : 1	1 : 1	2 : 1
Temperature [°C]	650–1000	400–1000	950–1100
Pressure, bar	1	3–40	1–100
Molar ratio of H_2/CO at the reactor outlet	1 : 1	3 : 1	2 : 1

The main problem of the catalysts utilized for DMR is their rather quick deactivation. As shown in the literature, the problem is due to the high temperature of the DMR process, which leads to coking as well as sintering of the support and active material. This issue is covered in several articles (Alipour et al., 2014; Aramouni et al., 2018; Bawadi et al., 2017; Benguerba et al., 2015; Borowiecki, 2006; Chein and Fung, 2019; Dębek et al., 2014; Richardson and Paripatayadar, 1990; Snoeck et al., 2002; Zambrano et al., 2019; Zhang et al., 2018), which present the state of the art in the field of catalysts dedicated to the DMR process. The above-mentioned investigations show that the nickel catalyst supported on Al_2O_3 carrier is the most widely used for the DMR process due to low cost and quite high specific surface area of the support. To increase activity of this catalyst and to prevent coking, other supports are also used. Moreover, various additives (promoters) are often introduced into the basic Al_2O_3 support for the same purpose. Undoubtedly, the method of preparing the catalysts also has a significant impact on their activity and stability under the process operating conditions.

The effect of MgO, CaO and BaO additions to unmodified Ni/Al_2O_3 catalyst on its activity was explored also by Alipour et al. (2014). A pronounced increase in the CH_4 and CO_2 conversion rates due to these additives was reported. Simultaneously, after approximately 6 hours of testing, neither a negative nor a positive effect of these additives on the catalysts stability was found. The highest increase of the catalyst activity was obtained for MgO. However, the impact of MgO addition was varied for a nickel catalyst having a higher nickel content (20% Ni). The use of the MgO modified catalyst with 20% of nickel showed a positive effect only on CO_2 conversion, while CH_4 conversion decreased.

An improved activity of a nickel catalyst was observed after the addition of cerium oxide (CeO_2) (Chein and Fung, 2019; Zambrano et al., 2019). Moreover, a reduced coking rate was detected. The optimal amount of CeO_2 was found, above which a decrease in the activity of the catalyst was observed as a result of the reduction of its specific surface area.

Furthermore, materials based on hydrotalcites (naturally occurring minerals with the formula $Mg_6Al_2(OH)_{16}CO_3 \cdot 4H_2O$) proved to be promising for the DMR process. They are also highly active and stable (Dębek et al., 2014).

Most of the published results refer to the catalysts fabricated in small quantities, which are sufficient for laboratory testing. Often the form of these catalysts (e.g. fine sieve fraction) is unsuitable for the use in an industrial scale. For this reason, the results of such studies can only help to indicate the methods of modification of commercial catalysts available on the market.

In industrial applications, other factors besides catalyst activity are also very important, i.e.: the cost of catalyst production, stability of the catalyst activity and mechanical strength.

Taking these aspects into account, it was decided that at the present stage of the project realization (project POIR.04.01.01-00-0064/18, 2019–2022) a commercial catalyst will be utilized for the syngas production. However, if needed, the catalyst can be modified in the future.

This paper presents the results of investigations into the DMR process that was carried out by using a commercial catalyst G-0217-7H/C produced by the Łukasiewicz Research Network – New Chemical Syntheses Institute in Puławy. The catalyst contains nickel deposited on a porous Al_2O_3 support with the addition of CaO to hinder coking. This catalyst is dedicated mainly to SMR, thus, the performed tests were aimed at checking its suitability in the DMR process.

2. EXPERIMENTAL

2.1. Setup and materials

The experimental setup used for the testing of the DMR process and its kinetics is shown in Fig. 1. The main components of the setup are described as follows.

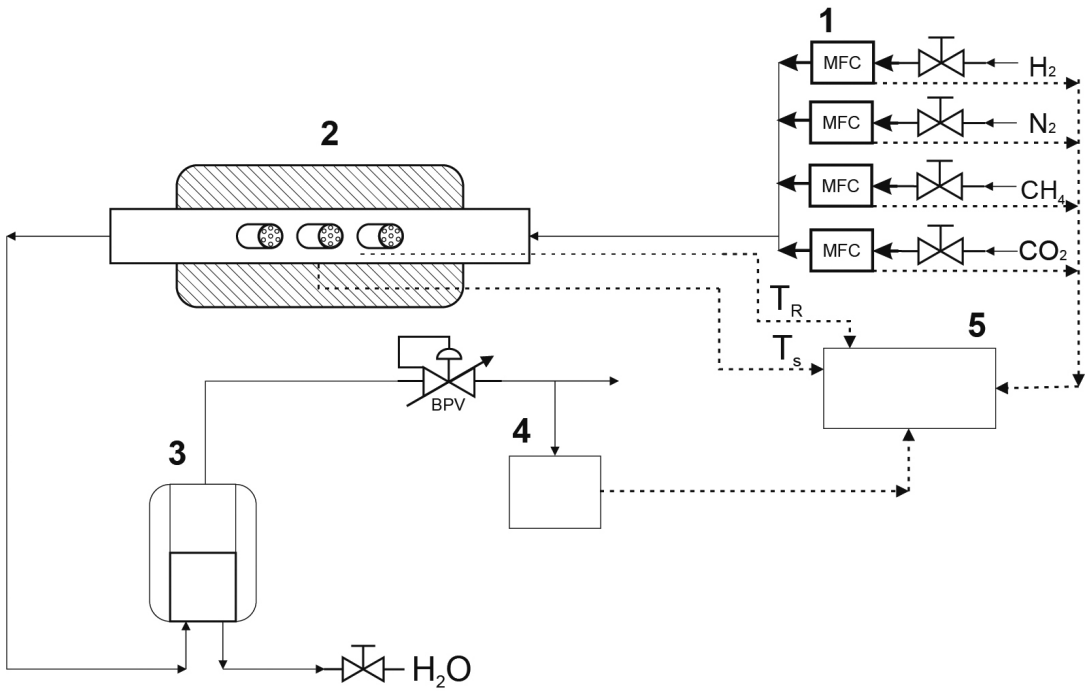

Fig. 1. Experimental setup for testing the DMR process; 1 – mass flow controllers, 2 – electric furnace with a tubular reactor, 3 – cooling system for gases leaving the reactor – water vapour condenser, 4 – gas analysis system, 5 – control and data acquisition system. MFC – mass flow controller, BPV – back pressure controller

2.1.1. Reactor

A tubular reactor with an internal diameter of 0.021 m and a working length of 0.400 m was used. The steel reactor was placed in a ceramic tube of a high-temperature electric furnace. The reactor was operated in a horizontal position. Due to the requirements of the DMR process, the reactor was maintained at a high temperature within the range of 480–888 °C during tests. A furnace temperature control system enabled us to obtain repeatable and stable operating conditions.

2.1.2. Gas flow and pressure control system

A separate module of the experimental system was used to control the gas flow and pressure in the reactor. The module was purchased from PPH Beta-Erg (Poland). It includes four mass flow regulators with microprocessor controllers, one back pressure regulator and dedicated software.

2.1.3. Steam condenser

The process gas was cooled and any water vapour that could be formed in the process was condensed before the gas pressure at the reactor outlet was reduced by the back pressure regulator. The equilibrium water vapour content in the gas leaving the condenser was determined from the known temperature of the condensate.

2.1.4. Catalyst

A commercial catalyst G-0217-7H/C produced by the Łukasiewicz Research Network – New Chemical Syntheses Institute in Puławy was used in the tests. The catalyst contains nickel deposited on a porous Al_2O_3 support with the addition of CaO. The minimum NiO content in the catalyst grains is 17% by mass, as specified by the producer. Prior to each series of the measurements, the catalyst was activated by hydrogen (reduction of NiO to Ni). The geometry of a single catalyst grain is shown in Fig. 2.

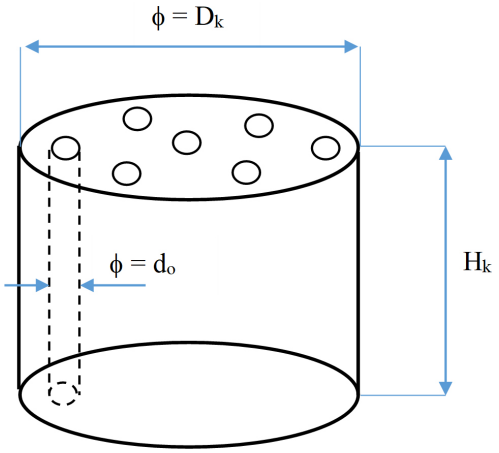

Fig. 2. Geometry of the G-0217-7H/C catalyst grain

The catalyst grain has a cylindrical shape with seven holes along the axis and slightly round bases (bottom and top). The height of the catalyst grain is $H_k \approx 0.018$ m and a diameter is $D_k \approx 0.0165$ m. Each of seven holes in the grain has a diameter of $d_o \approx 0.0034$ m. Such geometry provides a compact and permeable bed structure in a reformer. The catalyst bed is characterized by a low pressure drop and a relatively high ratio of the gas contact surface area to the catalyst grain volume.

The mean contact surface area of the catalyst grain with the gas is $F_k \approx 2.423 \cdot 10^{-3}$ m^2, and the averaged volume of the solid is $V_k \approx 2.484 \cdot 10^{-6}$ m^3. Hence, the grain characteristic size is $L_k \approx V_k/F_k \approx 1.025 \cdot 10^{-3}$ m.

The average mass of the catalyst grain is $m_k \approx 6.36$ g, thus, using the known particle volume, V_k, and the catalyst material density, ρ_s (assuming that it is approximately equal to the density of Al_2O_3, $\rho_s \approx 4.0$ g/cm^3), the approximate internal porosity of the catalyst particle can be determined, ε_k, from Eq. (1).

$$V_k\,(1-\varepsilon_k) = V_s = \frac{m_k}{\rho_s} \tag{1}$$

where V_s is the volume of the solid making up the grain.

Overall, the value of the internal porosity of the catalyst grain is $\varepsilon_k \approx 0.36$.

2.1.5. Analysis of the outlet gas composition

A gas microchromatograph (Fusion, USA) was used to analyse the composition of the gas leaving the reactor. Appropriate chromatographic programs were developed to measure simultaneously the content of hydrogen, nitrogen, methane, carbon monoxide and carbon dioxide in the outlet gas stream. Linear relationships were found between the chromatographic responses and gas concentrations for each compound over the concentration ranges studied.

2.2. Methods

The process conditions were determined by setting the following variables: concentration of each compound: CH_4, CO_2, N_2, H_2 in the inlet gas stream, temperature of the catalyst grain (T_R), and pressure in the reactor (P_R). For each measurement, the inlet and outlet gas stream compositions were determined after reaching a steady state. The active catalyst bed in the reactor consisted of one or four catalyst pellets. When four pellets were used, they were arranged in the reactor tube one after the other.

Whole (not crushed) catalyst grains were used in these tests. Such an approach allows the found kinetic relationships to be used directly to model the scale-up processes. However, one should keep in mind that generally the internal and external mass transfer resistances may be lumped into such kinetic relationships. This problem will be discussed in the next part of this paper.

In order to obtain reproducible catalyst operating conditions, catalyst reduction was performed before each measurement series. Then, a series of measurements were carried out for a fixed temperature by changing the inlet streams of gaseous substrates (reactant concentrations) or the total pressure. To widen the concentration ranges, some measurements were conducted with the addition of nitrogen to dilute the inlet stream of substrates.

3. RESULTS

The results of DMR tests are given in Tables 2–3. Table 2 details the results for the equimolar inlet gas streams, containing CH_4 and CO_2. Table 3 shows the results for the diluted inlet gas streams (nitrogen and varying amounts of CH_4 and CO_2). In some measurements, hydrogen was also added to the inlet gas stream.

Table 2. Process conditions for DMR carried out using the G-0217-7H/C catalyst. Equimolar ratios of CH_4 and CO_2 streams at the reactor inlet, reactor pressure P_R = 2 bar

No.	T_R [°C]	Volumetric flow rate at the reactor inlet [Nml/min]		Molar fractions of reagents at the reactor outlet [–]				Residence time τ [s]
		$Q_{o,1}$	$Q_{o,4}$	y_1	y_3	y_4	y_5	
		CH_4	CO_2	CH_4	H_2	CO_2	CO	
a) Four catalyst pellets – catalyst bed length L = 0.072 m								
1	480	200	200	0.46	0.04	0.46	0.04	1.11
2	480	25	25	0.42	0.09	0.44	0.05	8.86
3	480	50	50	0.43	0.07	0.44	0.05	4.43
4	583	100	100	0.22	0.30	0.31	0.13	1.95
5*	583	50	50	0.25	0.25	0.32	0.12	5.85
6	583	50	50	0.24	0.29	0.31	0.15	3.90
7	583	100	100	0.22	0.30	0.31	0.13	1.95
8	685	50	50	0.09	0.42	0.19	0.26	3.48
9	685	200	200	0.17	0.33	0.22	0.28	0.87
10	685	50	50	0.12	0.41	0.25	0.20	3.48
11	685	50	50	0.09	0.42	0.19	0.26	3.48
12	786	50	50	0.03	0.47	0.07	0.42	3.15
13	888	50	50	0.02	0.48	0.06	0.44	2.87
b) One catalyst pellet – catalyst bed length L = 0.018 m								
1	480	50	50	0.44	0.06	0.44	0.05	1.11
2	480	100	100	0.46	0.05	0.45	0.04	0.56
3	583	50	50	0.28	0.26	0.34	0.13	0.98
4	583	100	100	0.29	0.24	0.34	0.13	0.49

*measurement for P_R = 3 bar

Figures 3 and 4 show the results for the equimolar ratio of CH_4 and CO_2 in the inlet gas stream at the same pressure and comparable residence times of the reactants in the reactor. They show the effect of temperature on the reactant concentrations after the removal of water vapor (y_i), the conversion of CH_4 and CO_2 (ξ_{CH4} and ξ_{CO2}) and the molar fraction ratio of y_{CO} to y_{H2} in the outlet gas stream. These figures present the data summarized in Table 2a.

The conversions of CH_4 and CO_2 were calculated by using the following relationship

$$\zeta_i = \frac{\Phi_o y_{i,o} - \Phi y_i}{\Phi_o y_{i,o}} \tag{2}$$

A careful analysis of these results reveals that the desired conversion of CH_4 and CO_2 and the syngas composition are obtained only above 800 °C (Figures 3 and 4).

Table 3. Process conditions for DMR carried out using the G-0217-7H/C catalyst. Process conditions: the inlet gas stream contains various amounts of CH_4 and CO_2 diluted with nitrogen. Four catalyst pellets – catalyst bed length L = 0.072 m

No.	T_R [°C]	Volumetric flow rate at the reactor inlet [Nml/min]				Molar fractions of reagents at the reactor outlet [–]					Residence time τ [s]
		$Q_{o,1}$ CH_4	$Q_{o,3}$ H_2	$Q_{o,4}$ CO_2	$Q_{o,6}$ N_2	y_1 CH_4	y_3 H_2	y_4 CO_2	y_5 CO	y_6 N_2	
a) reactor pressure P_R = 2 bar											
1	480	10	0	10	80	0.07	0.04	0.09	0.02	0.78	4.43
2	480	40	0	40	20	0.33	0.06	0.35	0.03	0.22	
3	480	30	0	30	40	0.23	0.05	0.26	0.02	0.43	
4	480	20	0	20	60	0.14	0.04	0.17	0.02	0.62	
5	480	10	0	10	80	0.06	0.03	0.08	0.02	0.80	
6	480	10	10	10	70	0.10	0.05	0.08	0.02	0.75	
7	583	10	0	10	80	0.02	0.10	0.06	0.06	0.77	3.90
8	583	40	0	40	20	0.17	0.24	0.24	0.13	0.22	
9	583	30	0	30	40	0.12	0.20	0.18	0.11	0.40	
10	583	20	0	20	60	0.07	0.15	0.12	0.08	0.58	
11	583	10	0	10	80	0.02	0.09	0.05	0.06	0.77	
12	583	10	10	10	70	0.05	0.13	0.05	0.06	0.71	
13	685	10	0	10	80	0.01	0.12	0.05	0.10	0.72	3.48
14	685	40	0	40	20	0.07	0.35	0.16	0.23	0.18	
15	685	30	0	30	40	0.05	0.28	0.12	0.19	0.35	
16	685	20	0	20	60	0.03	0.20	0.09	0.15	0.53	
17	685	10	0	10	80	0.01	0.11	0.05	0.09	0.72	
18	685	10	10	10	70	0.03	0.16	0.05	0.09	0.67	
19	685	10	0	10	80	0.01	0.14	0.05	0.09	0.71	
20	685	10	10	10	70	0.02	0.20	0.05	0.10	0.62	
21	786	10	0	10	80	0.00	0.14	0.02	0.16	0.68	3.15
22	786	40	0	40	20	0.02	0.41	0.06	0.38	0.13	
23	786	30	0	30	40	0.01	0.33	0.04	0.34	0.28	
24	786	20	0	20	60	0.01	0.25	0.02	0.27	0.45	
25	786	10	0	10	80	0.00	0.14	0.01	0.17	0.68	
26	786	10	10	10	70	0.01	0.20	0.01	0.18	0.60	
27	888	30	0	50	20	0.01	0.32	0.14	0.39	0.14	2.87
28	888	60	0	20	20	0.04	0.63	0.03	0.15	0.14	
29	888	20	0	60	20	0.00	0.21	0.17	0.48	0.14	
30	888	50	0	30	20	0.02	0.52	0.05	0.27	0.14	
31	888	30	0	50	20	0.01	0.31	0.10	0.45	0.13	
32	888	10	10	10	70	0.00	0.21	0.02	0.16	0.61	
33	888	10	0	10	80	0.00	0.15	0.03	0.15	0.67	
34	888	40	0	40	20	0.01	0.41	0.04	0.41	0.13	
35	888	30	0	30	40	0.01	0.34	0.03	0.35	0.27	
36	888	20	0	20	60	0.00	0.25	0.02	0.29	0.44	
37	888	10	0	10	80	0.00	0.14	0.01	0.19	0.66	
38	888	10	10	10	70	0.00	0.22	0.01	0.19	0.58	

Table 3 [cont.]

No.	T_R [°C]	Volumetric flow rate at the reactor inlet [Nml/min]				Molar fractions of reagents at the reactor outlet [–]					Residence time τ [s]
		$Q_{o,1}$ CH_4	$Q_{o,3}$ H_2	$Q_{o,4}$ CO_2	$Q_{o,6}$ N_2	y_1 CH_4	y_3 H_2	y_4 CO_2	y_5 CO	y_6 N_2	
b) reactor pressure P_R = 3 bar											
1	685	10	0	10	80	0.01	0.15	0.07	0.08	0.69	5.22
2	685	40	0	40	20	0.10	0.35	0.19	0.18	0.18	
3	685	30	0	30	40	0.07	0.28	0.15	0.16	0.35	
4	685	20	0	20	60	0.03	0.21	0.10	0.12	0.54	
5	685	10	0	10	80	0.01	0.13	0.05	0.09	0.73	

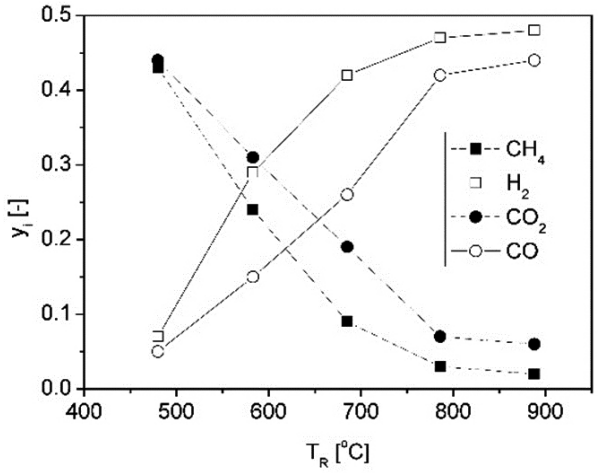

Fig. 3. Effect of temperature on reactant concentrations in the outlet gas stream

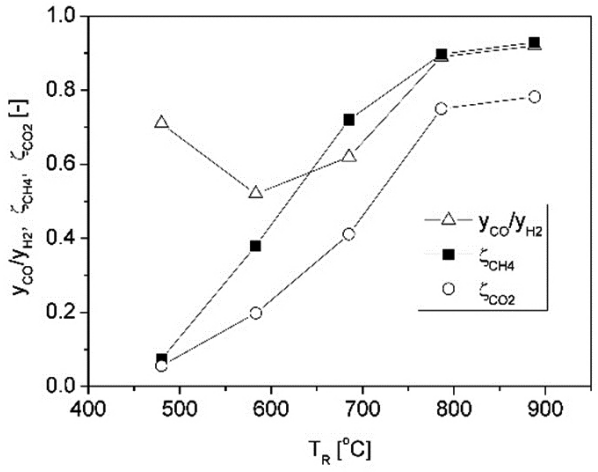

Fig. 4. Effect of temperature on the conversion of the substrates (CH_4 and CO_2) and the y_{CO}/y_{H2} ratio in the outlet gas stream

Figure 5 shows the effect of the inlet gas stream composition, i.e. the molar fraction ratio of CH_4 to CO_2 ($y_{CH4,0}/y_{CO2,0}$), on the conversion of the both compounds (results are based on the data in Table 3). As can be seen in Fig. 5, the excess carbon dioxide in the inlet gas stream (i.e. values of the ratio $y_{CH4,0}/y_{CO2,0}$ lower

than one) causes the methane conversion to be close to one and the CO_2 conversion to be unsatisfactory. Increasing the $y_{CH4,0}/y_{CO2,0}$ ratio results in an increase of the CO_2 conversion and a slight decrease in the CH_4 conversion.

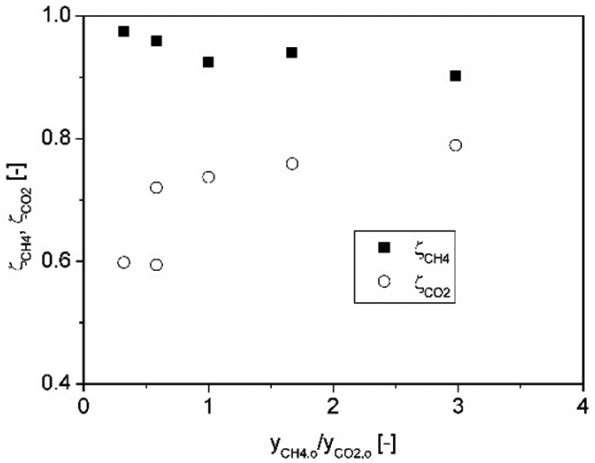

Fig. 5. Effect of the inlet gas composition ($y_{CH4,0}/y_{CO2,0}$) on the CH_4 and CO_2 conversions. Process conditions: T_R = 888 °C, P_R = 2 bar, y_{N2} = 0.2

Figure 6 shows the effect of the $y_{CH4,0}/y_{CO2,0}$ ratio on the syngas composition, i.e. the molar ratio of CO to H_2. The desired molar ratio of CO to H_2 (close to one) in the syngas is obtained for the following ratio $y_{CH4,0}/y_{CO2,0} \approx 0.7 - 0.8$. Increasing and decreasing this value causes significant deviations from the desired ratio of CO to H_2. Note, however, that for the following ratio $y_{CH4,0}/y_{CO2,0} \approx 0.7$–0.8 the CH_4 conversion is about 0.95, while the CO_2 conversion is only 0.6–0.7.

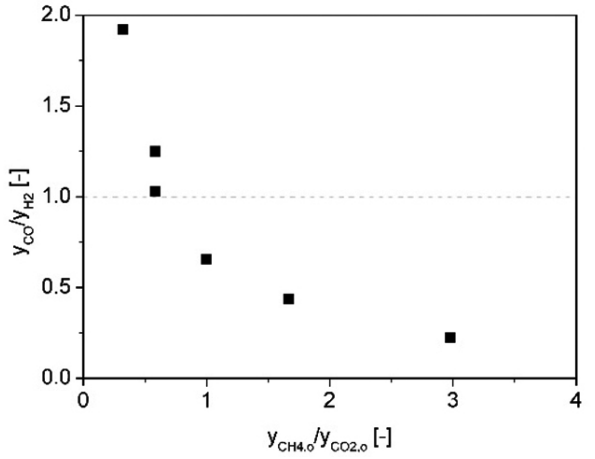

Fig. 6. Effect of the inlet gas composition ($y_{CH4,0}/y_{CO2,0}$) on the syngas composition (y_{CO}/y_{H2}). Process conditions: T_R = 888 °C, P_R = 2 bar, y_{N2} = 0.2

The assessment of the data presented in Figs. 5 and 6 is of great importance for the design of the DMR process operating conditions and the optimization of the process to obtain syngas for DME production.

As shown in the literature (Alipour et al., 2014; Bawadi et al., 2017; Benguerba et al., 2015; Borowiecki, 2006; Dębek et al., 2014), carrying out the DMR process at high temperatures may lead to coking and deactivation of the catalyst. With this in mind the activity of the catalyst was monitored in each measurement series (for each temperature) in such a way that the first measurement in the series was repeated at its end. Figure 7 compares the first and last results in the series for the data summarized in Table 3.

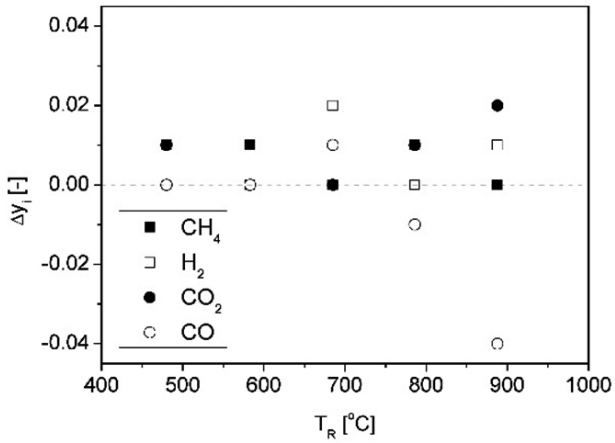

Fig. 7. Reproducibility of results for each compound. The effect of temperature on the difference in concentrations between the first and last measurement in the measurement series, Δy_i

Figure 7 reveals that there is no clear decrease in the catalyst activity (also for the highest temperature of $T_R = 888\,^{\circ}\mathrm{C}$), i.e. changes in the concentrations of individual reagents after the first and last measurements in the series are within the accuracy of concentration measurements.

A noticeable difference was observed only for CO at the highest temperature ($\Delta y_{CO} = 0.04$). The observed stability of the G-0217-7H/C catalyst activity may indicate that the presence of CaO in the catalyst hinder the production of carbon deposits.

In the further part of the work, a method of describing the DMR kinetics is proposed, taking into account the formation of carbon deposits.

4. MODELLING OF REACTION KINETICS IN DMR PROCESS

4.1. System of chemical reactions for DMR

The reaction kinetics of DMR can be represented by a system of the following chemical reactions (Benguerba et al., 2015; Zambrano et al., 2019):

$$CH_4 + CO_2 \leftrightarrow 2CO + H_2 \qquad \Delta H = 247\ \mathrm{kJ/mol} \tag{3}$$

$$CO_2 + H_2 \leftrightarrow CO + H_2O \qquad \Delta H = 41.7\ \mathrm{kJ/mol} \tag{4}$$

In addition to the main reaction (3), the reaction (4) is considered, which is the reverse to the water-gas shift reaction. Note that both the reactions (3)–(4) are endothermic, and that reaction (3) increases of the reaction mixture volume, what results in an increase of the volumetric and molar flow rates of the gas stream in the reactor.

The catalyst coking is a significant problem accompanying the production of syngas by DMR. This can lead to the deactivation of the catalyst. This problem occurs especially in the case of high temperature and the presence of significant amounts of CO_2 in the feed stream. The problem is widely described in the literature, e.g. (Alipour et al., 2014; Aramouni et al., 2018; Bawadi et al., 2017; Benguerba et al., 2015; Borowiecki, 2006; Chein and Fung, 2019; Dębek et al., 2014; Zambrano et al., 2019; Zhang et al., 2018).

The following reaction scheme was proposed by Benguerba et al. (2015) to describe the formation of carbon deposits and their further conversion.

$$CH_4 \leftrightarrow C_{(s)} + 2H_2 \qquad \Delta H = 74.9\ \mathrm{kJ/mol} \tag{5}$$

$$C_{(s)} + H_2O \leftrightarrow CO + H_2 \qquad \Delta H = 131.3 \text{ kJ/mol} \tag{6}$$

$$C_{(s)} + CO_2 \leftrightarrow 2CO \qquad \Delta H = 172 \text{ kJ/mol} \tag{7}$$

The above Eqs. (3)–(7) indicate that they are crucial to model the DMR process in a proper way, as all of them have an impact of the syngas composition.

4.2. Kinetic model

One of the methods of modelling the DMR reaction kinetics was proposed by Benguerba et al. (2015). According to this method, the rate of chemical reactions, r_{I}, r_{II}, r_{III}, r_{IV}, r_{V}, shown in Eqs. (3)–(7) are calculated from the following kinetic relationships:

$$r_{\mathrm{I}} = \frac{k_{\mathrm{I}}\, p_{\mathrm{CH4}}\, p_{\mathrm{CO2}}\, K_{\mathrm{CH4,I}}\, K_{\mathrm{CO2,I}}}{\left(1 + K_{\mathrm{CO2,I}}\, p_{\mathrm{CO2}} + K_{\mathrm{CH4,I}}\, p_{\mathrm{CH4}}\right)^2} \left(1 - \frac{\left(p_{\mathrm{CO}}\, p_{\mathrm{H2}}\right)^2}{K_{\mathrm{P,I}}\left(p_{\mathrm{CH4}}\, p_{\mathrm{CO2}}\right)}\right) \tag{8}$$

$$r_{\mathrm{II}} = \frac{k_{\mathrm{II}}\, p_{\mathrm{H2}}\, p_{\mathrm{CO2}}\, K_{\mathrm{H2,II}}\, K_{\mathrm{CO2,II}}}{\left(1 + K_{\mathrm{CO2,II}}\, p_{\mathrm{CO2}} + K_{\mathrm{H2,II}}\, p_{\mathrm{H2}}\right)^2} \left(1 - \frac{\left(p_{\mathrm{CO}}\, p_{\mathrm{H2O}}\right)}{K_{\mathrm{P,II}}\left(p_{\mathrm{CO2}}\, p_{\mathrm{H2}}\right)}\right) \tag{9}$$

$$r_{\mathrm{III}} = \frac{k_{\mathrm{III}}\, K_{\mathrm{CH4,III}} \left(p_{\mathrm{CH4}} - \dfrac{p_{\mathrm{H2}}^2}{K_{p,\mathrm{III}}}\right)}{\left(1 + K_{\mathrm{CH4,III}}\, p_{\mathrm{CH4}} + \dfrac{p_{\mathrm{H2}}^{1.5}}{K_{\mathrm{H2,III}}}\right)^2} \tag{10}$$

$$r_{\mathrm{IV}} = \frac{\dfrac{k_{\mathrm{IV}}}{K_{\mathrm{H2O,IV}}} \left(\dfrac{p_{\mathrm{H2O}}}{p_{\mathrm{H2}}} - \dfrac{p_{\mathrm{CO}}}{K_{p,IV}}\right)}{\left(1 + K_{\mathrm{CH4,IV}}\, p_{\mathrm{CH4}} + \dfrac{p_{\mathrm{H2O}}}{K_{\mathrm{H2O,IV}}\, p_{\mathrm{H2}}} + \dfrac{p_{\mathrm{H2}}^{1.5}}{K_{\mathrm{H2,IV}}}\right)^2} \tag{11}$$

$$r_{\mathrm{V}} = \frac{\dfrac{k_{\mathrm{V}}}{K_{\mathrm{CO,V}} K_{\mathrm{CO2,V}}} \left(\dfrac{p_{\mathrm{CO2}}}{p_{\mathrm{CO}}} - \dfrac{p_{\mathrm{CO}}}{K_{p,V}}\right)}{\left(1 + K_{\mathrm{CO,V}}\, p_{\mathrm{CO}} + \dfrac{p_{\mathrm{CO2}}}{K_{\mathrm{CO,V}}\, K_{\mathrm{CO2,V}}\, p_{\mathrm{CO}}}\right)^2} \tag{12}$$

The values of the constants appearing in the kinetic Eqs. (8)–(12) and their dependence on the temperature are the subject of the analysis presented below.

4.3. Reactor model

In order to find the values of the constants appearing in the kinetic relationships (8)–(12), calculations were carried out using our own experimental results shown in Tables 2 and 3.

Modelling of methane reforming process carried out in the packed bed reactors is quite widely described in the literature of subject, however mostly the steam methane reforming process – also sorption enhanced one – is considered. For both types of processes, dry methane and steam methane reforming, the following papers should be mentioned, which presented conceptual approach to process modelling as well as values of the transport and physico-chemical parameters: Ding and Alpay (2000); Xiu et al. (2003); Wang and Rodrigues (2005); Oliveira et al. (2009); Oliveira et al. (2010); Halabi et al. (2012); Chanburanasiri et al. (2013); Farniaei et al. (2014) and Zambrano et al. (2020).

In our studies the following assumptions were made to develop the reactor model:

- the reactor is isothermal (T_R = const.) and isobaric (P_R = const.),
- the flow of the gas mixture through the catalyst bed is treated as a plug flow,
- the axial dispersion of mass and heat in the reactor bed can be neglected,
- the pressure drop due to the gas flow through the catalyst bed may be neglected,
- the gas mixture behaves as an ideal gas,
- the effect of external mass transfer resistances can be neglected, while the internal mass transfer resistances are taken into account,
- uniform temperature distribution within the catalyst grain can be assumed.

These assumptions result from the reactor geometry, the shape of the catalyst grain and the method of performing the process.

As shown in the experimental section above, the characteristic dimension of the catalyst grain is as small as $L_k \approx 1.025 \cdot 10^{-3}$ m. Because of this as well as due to a relatively high thermal conductivity of the catalyst carrier, which at the process temperature is within the range of $\lambda_{Al_2O_3} \approx 8 \div 10$ [W/m K], the uniform temperature distribution within the solid phase can be assumed. This assumption was successively justified performing CFD simulations for a single catalyst pellet and the DMR reactions. These simulations were carried out at the most severe conditions – i.e. at the highest temperature (T_R = 900 °C) and for reaction carried out at the pellet surface. For this purposes the intrinsic kinetics data for DMR reactions determined by Benguerba et al. (2015) was utilized. The obtained uniform temperature distribution within the catalyst pellet indicates that the temperature (T_R) measured directly at the pellet surface is the process temperature and there is no need to take into account heat transfer resistances for the reactor wall-catalyst grain surface system.

Because the internal mass transfer resistances control the process rate, it was assumed that the external mass transfer resistances can be neglected. A significance of the internal diffusion for each j-th elementary reaction (see Eqs. (3)–(7)) was quantitatively estimated with the overall catalyst effectiveness factor η_j.

Given that the catalyst grain has a cylindrical shape with seven holes along the axis, the pressure drop along the catalyst bed, formed by one or four grains, can be neglected.

The following indexing has been introduced for the reagents:

1 – CH_4 | 2 – H_2O | 3 – H_2 | 4 – CO_2 | 5 – CO | 6 – N_2

On the basis of the stoichiometric Eqs. (3)–(7), the conversion rates of each reactant, $r_{R,i}$, can be related to the rates of reactions (8)–(12) to obtain the following:

$$r_{R,1} = -\eta_{\mathrm{I}} r_{\mathrm{I}} - \eta_{\mathrm{III}} r_{\mathrm{III}} \tag{13}$$

$$r_{R,2} = \eta_{\mathrm{II}} r_{\mathrm{II}} - \eta_{\mathrm{IV}} r_{\mathrm{IV}} \tag{14}$$

$$r_{R,3} = 2\eta_{\mathrm{I}} r_{\mathrm{I}} - \eta_{\mathrm{II}} r_{\mathrm{II}} + 2\eta_{\mathrm{III}} r_{\mathrm{III}} + \eta_{\mathrm{IV}} r_{\mathrm{IV}} \tag{15}$$

$$r_{R,4} = -\eta_{\mathrm{I}} r_{\mathrm{I}} - \eta_{\mathrm{II}} r_{\mathrm{II}} - \eta_{\mathrm{V}} r_{\mathrm{V}} \tag{16}$$

$$r_{R,5} = 2\eta_{\mathrm{I}} r_{\mathrm{I}} + \eta_{\mathrm{II}} r_{\mathrm{II}} + \eta_{\mathrm{IV}} r_{\mathrm{IV}} + 2\eta_{\mathrm{V}} r_{\mathrm{V}} \tag{17}$$

where η_j is the catalyst effectiveness factor for each j-th elementary reaction I÷V (Eqs. (13)–(17)).

Then, in a steady state, the molar balance for each i-th component in the reactor can be written as follows:

$$-\frac{\mathrm{d}}{\mathrm{d}x}(\Phi y_i) + r_{R,i}\frac{m_K}{L} = 0 \tag{18}$$

where the conversion rate of the i-th reactant, $r_{R,i}$, can be calculated using the relationships (13)–(17) and the kinetic equations (8)–(12).

The mathematical model also employs the following equation

$$p_i = y_i \cdot P_R \tag{19}$$

which relates the reactant partial pressures to their molar fractions in the gas mixture, and the general molar balance for the reactor

$$\frac{\mathrm{d}\Phi}{\mathrm{d}x} = \sum_{i=1}^{5} \left(r_{R,i} \frac{m_K}{L} \right) \tag{20}$$

Given that the process was carried out under isothermal conditions, the heat balance equation was not included in the model.

The model equations (13)–(20) were implemented in the MatLab environment. The use of numerical procedures contained in this software allows for high computation speed, good convergence and accuracy. The purpose of the model calculations was to verify the literature kinetic relationships presented by Benguerba et al. (2015).

4.4. Model calculations and the verification of kinetic relationships

It was assumed that the system of chemical reactions (3)–(7) with the kinetic relationships (8)–(12) correctly describes the DMR processes. The system of model equations was solved using the experimental data summarized in Tables 2 and 3, i.e. for the listed temperatures, T_R, total pressures, P_R, lengths of the catalyst bed, L, and the inlet gas concentrations, $y_{i,o}$.

The calculation results, being the reactant concentrations in the outlet gas stream, $y_{i,\mathrm{mod}}$, were compared with the experimental results, $y_{i,\mathrm{exp}}$.

With the kinetic and adsorption constants taken directly from the studies of Benguerba et al. (2015), a good agreement between the modelling and experimental results was obtained for the products – H_2 and CO, while significant and systematic deviations were observed for the substrates, especially for CH_4. It is not even surprised, as the crushed catalyst of diameter of $d_p = 0.4$ mm was used in the cited paper, while whole pellets was utilized in our studies.

Taking into account that for the considered system, the reaction rate constants appearing in the rate expressions (Eqs. (8)–(12)): $k_\mathrm{I} - k_\mathrm{V}$ and the appropriate catalyst effectiveness factors: $\eta_\mathrm{I} - \eta_\mathrm{V}$ are both only the temperature function, in the next step the following approach was adopted. In model calculations, using our own experimental data, the apparent rate constant – $k_{j,\mathrm{app}}$ (being the product of both mentioned above parameters $k_{j,\mathrm{app}} = \eta_j \cdot k_j$) was estimated, while the adsorption constants $K_{i,j}$ (for i-th reactant and j-th reaction, respectively) and the reaction equilibrium constants $K_{p,j}$ (for j-th recation) was taken directly from the work of Benguerba et al. (2015).

The applied approach makes possible modelling the reaction rates in the considered system, however one has to keep in mind that determined values of the apparent rate constants – $k_{j,\mathrm{app}}$ are only valid for the catalyst pellets used in presented experiments. But mentioned values can be utilized to model the reactor in which various bed configurations are formed with these pellets.

New calculations series were performed to estimate the apparent rate constants. Using the problem-based nonlinear least squares approach in the Matlab Optimization Toolbox, it was found that the modelling results satisfactorily reflects the experimental data.

Table 4 presents the complete set of kinetic and adsorption constants obtained for the utilized catalyst G-0217-7H/C.

Table 4. Kinetic, adsorption and equilibrium constants of the DMR reaction along with their dependence on temperature. (The values of the constants appearing in this table are chosen in such a way to obtain the values of the reaction rates $r_I - r_V$ in (mol $kg_{cat}^{-1}s^{-1}$) after inserting these constants into the kinetic equations (8)–(12). Reagent partial pressures, p_i, are expressed in bars.)

Parameter	Equation	Parameter	Equation
Apparent rate constants $k_{j,app} = \eta_j \cdot k_j$ adjusted for the used G-0217-7H/C catalyst			
$k_{I,app}$	$1.74 \cdot 10^7 \exp\left(\frac{-102065}{RT}\right)$	$k_{IV,app}$	$1.11 \cdot 10^9 \exp\left(\frac{-166397}{RT}\right)$
$k_{II,app}$	$9.08 \cdot 10^4 \exp\left(\frac{-81030}{RT}\right)$	$k_{V,app}$	$1.16 \cdot 10^{14} \exp\left(\frac{-243835}{RT}\right)$
$k_{III,app}$	$7.85 \cdot 10^1 \exp\left(\frac{-58893}{RT}\right)$		
Adsorption and reaction equilibrium constants taken from (Benguerba et al., 2015)			
$K_{CO_2,I}$	$2.61 \cdot 10^{-2} \exp\left(\frac{37641}{RT}\right)$	$K_{H_2,IV}$	$1.83 \cdot 10^{13} \exp\left(\frac{-216145}{RT}\right)$
$K_{CH_4,I}$	$2.60 \cdot 10^{-2} \exp\left(\frac{40684}{RT}\right)$	$K_{CO,V}$	$7.34 \cdot 10^{-6} \exp\left(\frac{100395}{RT}\right)$
$K_{CO_2,II}$	$0.5771 \exp\left(\frac{9262}{RT}\right)$	$K_{CO_2,V}$	$2.81 \cdot 10^7 \exp\left(\frac{-104085}{RT}\right)$
$K_{H_2,II}$	$1.494 \exp\left(\frac{6025}{RT}\right)$	$K_{p,I}$	$6.78 \cdot 10^{14} \exp\left(\frac{-259660}{RT}\right)$
$K_{CH_4,III}$	$0.21 \exp\left(\frac{-567}{RT}\right)$	$K_{p,II}$	$56.4971 \exp\left(\frac{-36580}{RT}\right)$
$K_{H_2,III}$	$5.18 \cdot 10^7 \exp\left(\frac{-133210}{RT}\right)$	$K_{p,III}$	$2.98 \cdot 10^5 \exp\left(\frac{-84400}{RT}\right)$
$K_{H_2O,IV}$	$4.73 \cdot 10^{-6} \exp\left(\frac{97770}{RT}\right)$	$K_{p,IV}$	$1.3827 \cdot 10^7 \exp\left(\frac{-125916}{RT}\right)$
$K_{CH_4,IV}$	3.49	$K_{p,V}$	$1.9393 \cdot 10^9 \exp\left(\frac{-168527}{RT}\right)$

Figures 8–11 show a comparison of the experimental and modelling results for the case in which the verified kinetic relationships shown in table 4 were applied. The comparison is presented for all measurements

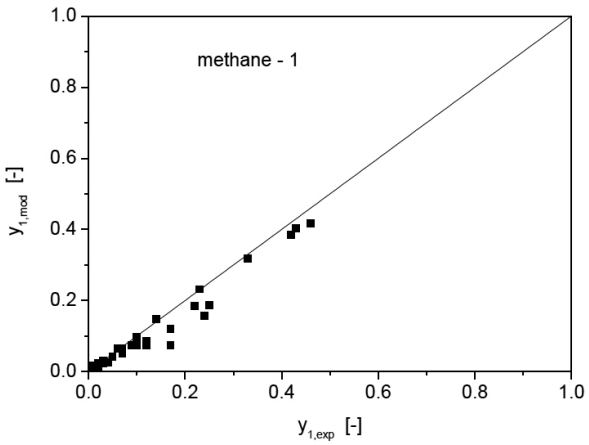

Fig. 8. Comparison of the experimental and modelling results for the CH_4 concentration in the outlet gas stream. Data for all measurements listed in Tables 2 and 3

summarized in Tables 2 and 3. As can be seen in Figures 8–11, there is a satisfactory fit of the results. Significant deviations are only observed for a few measurements. With this in mind and taking into account that the experiments were carried out over a wide range of temperatures, substrate concentrations and

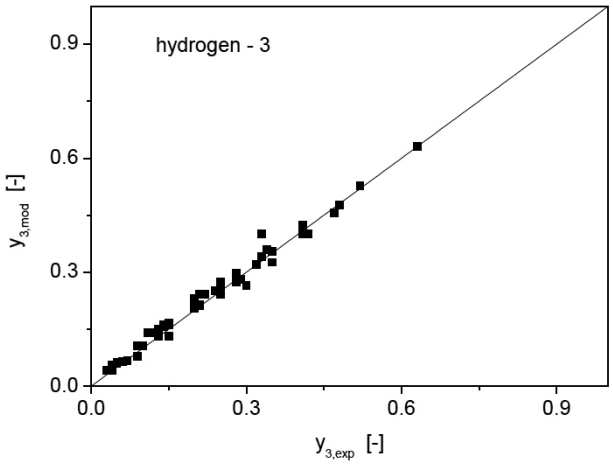

Fig. 9. Comparison of the experimental and modelling results for the H_2 concentration in the outlet gas stream. Data for all measurements listed in Tables 2 and 3

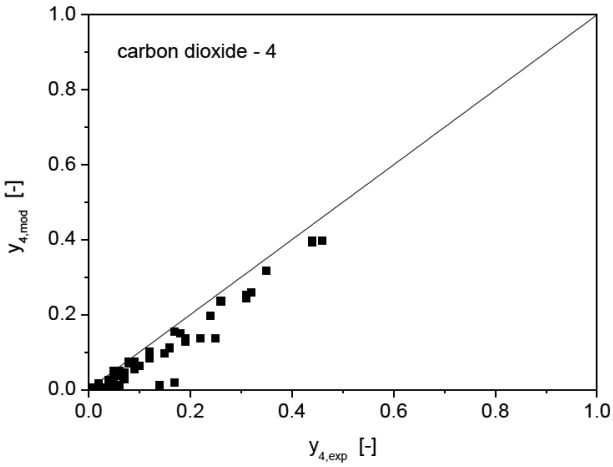

Fig. 10. Comparison of the experimental and modelling results for the CO_2 concentration in the outlet gas stream. Data for all measurements listed in Tables 2 and 3

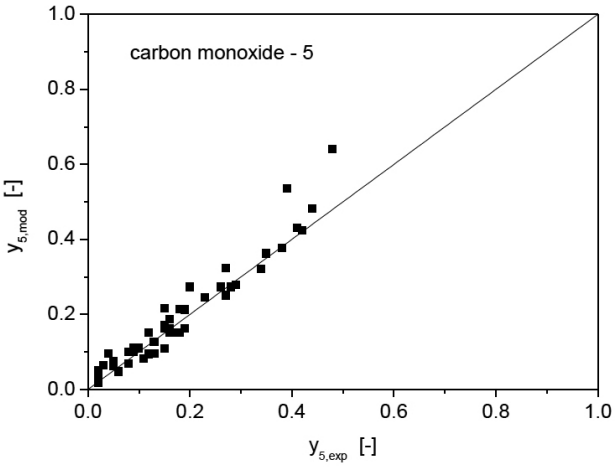

Fig. 11. Comparison of the experimental and modelling results for the CO concentration in the outlet gas stream. Data for all measurements listed in Tables 2 and 3

residence times, it can be concluded that the kinetic expressions presented in Table 4 describe the DMR process carried out on the G-0217-7H/C catalyst sufficiently well.

5. SUMMARY AND CONCLUSIONS

This work investigates the possible use of the G-0217-7H/C catalyst in the DMR process in the context of syngas production, which is the feedstock for DME synthesis.

Several series of measurements were carried out for the explored DMR process. The effect of the operating variables as: temperature, pressure, residence time and composition of the inlet gas stream were tested.

On the basis of 60 measurements, the examined G-0217-7H/C catalyst was found to be suitable in the DMR process. The influence of the above-mentioned operational variables on the DMR process was analysed, showing the range of parameter values which lead to the desired composition of syngas.

The reactor model was developed and the literature kinetic relationships were verified. The proposed reactor model and the adjusted kinetic relationships for the G-0217-7H/C catalyst have been proved to be appropriate for describing the DMR process with a satisfactory accuracy.

On the basis of performed tests and calculations, it was found that the presence of CaO in the G-0217-7H/C catalyst support hinders the catalyst coking.

As the experiments showed, no significant deactivation of the catalyst was found during the measurements lasting up to 6 hours. However, further work is required for the scale-up DMR process to check possible coking at high temperatures and the catalyst deactivation rate.

SYMBOLS

L	length of catalyst bed, ;m
k_j	reaction rate constant for j-th reaction, (units as in Table 4)
$k_{j,\mathrm{app}} = \eta_j \cdot k_j$	apparent reaction rate constant for j-th reaction, (units as in Table 4)
$K_{i,j}$	adsorption constants for i-th reactant and j-th reaction, respectively, (units as in Table 4)
$K_{p,j}$	reaction equilibrium constants for j-th reaction, (units as in Table 4)
m_K	catalyst mass in the reactor, kg
p_i	partial pressure of the i-th reactant, bar
P_R	reactor pressure, bar
$Q_{0,i}$	volumetric flow rate of the i-th reactant at the reactor inlet, Nml/min
T_R	temperature of the catalyst grain, °C
$r_{R,i}$	conversion rate of the i-th reactant, mol/($\mathrm{kg_{cat}}$ s)
$r_\mathrm{I} - r_\mathrm{V}$	reaction rates based on the stoichiometric equations (8)–(12), mol/($\mathrm{kg_{cat}}$ s)
$y_{0,i}$	molar fraction of the i-th reactant in the inlet gas stream, –
y_i	molar fraction of the i-th reactant in the reactor, –

Greek symbols

η_j	catalyst effectiveness factor for each j-th elementary reaction $I \div V$ (Eqs. (3)–(7)), –
τ	residence time in the reaction zone (related to the inlet flow rate, i.e. without taking into account the gas expansion due to chemical reaction), s

Φ	molar flow rate in the reactor, mol/s
Φ_0	molar flow rate at the reactor inlet, mol/s

ACKNOWLEDGMENTS

This research was carried out under the project POIR.04.01.01-00-0064/18 entitled *Development of technology for production of DME to utilize small sources of hydrocarbons*, financed by the National Center for Research and Development and PGNiG, 2019-2022.

The catalyst for the tests was provided free of charge by the producer: Łukasiewicz Research Network – New Chemical Syntheses Institute in Puławy – internet address: http://www.ins.lukasiewicz.gov.pl/index.php/en/products/catalysts-and-sorbents/hydrocarbon-steam-reforming

REFERENCES

Alipour Z., Rezaei M., Meshkani F., 2014. Effects of support modifiers on the catalytic performance of Ni/Al_2O_3 catalyst in CO_2 reforming methane. *Fuel*, 129, 197–203. DOI: 10.1016/j.fuel.2014.03.045.

Aramouni N.A.K., Touma J.G., Tarboush B.A., Zeaiter J., Ahmad M.N., 2018. Catalyst design for dry reforming of methane: Analysis review. *Renewable Sustainable Energy Rev.*, 82, 2570–2585. DOI: 10.1016/j.rser.2017.09.076.

Bawadi A., Nur Azeanni A.G., Dai-Vet N.V., 2017. Recent advances in dry reforming of methane over Ni-based catalysts. *J. Cleaner Prod.*, 162, 170–185. DOI: 10.1016/j.jclepro.2017.05.176.

Benguerba Y., Dehimi L., Virginie M., Dumas C., Ernst B., 2015. Modelling of methane dry reforming over Ni/Al_2O_3 catalyst in a fixed bed catalytic reactor. *Reac. Kinet. Mech. Cat.*, 114, 109–119. DOI: 10.1007/s11144-014-0772-5.

Borowiecki T., 2006. Coking of catalysts in essential chemical processes. *Przem. Chem.*, 85, 699–702.

Borowiecki T., Gołębiowski A., 2005. Modern synthesis gas and hydrogen plants. *Przem. Chem.*, 84, 503–507.

Chanburanasiri N., Ribeiro A.M., Rodrigues A.E., Laosiripojana N., Assbumrungrat S., 2013. Simulation of methane steam reforming enhanced by *in situ* CO_2 sorption utilizing K_2CO_3 promoted hydrotalcites for H_2 production. *Energy Fuels* 27, 4457–4470. DOI: 10.1021/ef302043e.

Chein R.Y., Fung W.Y., 2019. Syngas production via dry reforming of methane over CeO_2 modified Ni/Al_2O_3 catalysts. *Int. J. Hydrogen Energy*, 44, 14303–14315. DOI: 10.1016/j.ijhydene.2019.01.113.

Collodi G., Wheeler F., 2010. Hydrogen production via steam reforming with CO_2 capture. *Chem. Eng. Trans.*, 19, 37–42. DOI: 10.3303/CET1019007.

Dębek R., Gramatyka A., Motak M., da Costa P., 2014. Syngas production by dry reforming of methane over hydrotalcite-derived catalysts. *Przem. Chem.*, 93, 2026–2032.

Ding Y., Alpay E., 2000. Adsorption-enhanced steam-methane reforming. *Chem. Eng. Sci.*, 55, 39–3940. DOI: 10.1016/S0009-2509(99)00597-7.

Enger B.C., Lødeng R., Holmen A., 2008. A review of catalytic partial oxidation of methane to synthesis gas with emphasis on reaction mechanisms over transition metal catalysts. *Appl. Catal.*,*A*, 346, 1–27. DOI: 10.1016/j.apcata.2008.05.018.

Farniaei M., Abbasi M., Rahnama H., Rahimpour M.R., Shariatic A., 2014. Syngas production in a novel methane dry reformer by utilizing of tri-reforming process for energy supplying: Modeling and simulation. *J. Nat. Gas Sci. Eng*., 20, 132–146. DOI: 10.1016/j.jngse.2014.06.010.

Halabi M.H., de Croon M.H.J.M., van der Schaaf J., Cobden P.D., Schouten J.C., 2012. Kinetic and structural requirements for a CO_2 adsorbent in sorption enhanced catalytic reforming of methane – Part I: Reaction kinetics and sorbent capacity. *Fuel*, 99, 154–164. DOI: 10.1016/j.fuel.2012.04.016.

Oliveira E.L.G., Grande C.A., Rodrigues A.E., 2009. Steam methane reforming in a Ni/Al_2O_3 catalyst: Kinetics and diffusional limitations in extrudates. *Can. J. Chem. Eng.*, 87, 945–956. DOI: 10.1002/cjce.20223.

Oliveira E.L.G., Grande C.A., Rodrigues A.E., 2010. Methane steam reforming in large pore catalyst. *Chem. Eng. Sci.*, 65, 1539–1550. DOI: 10.1016/j.ces.2009.10.018.

Pena M., Gómez J., Fierro J.L.G., 1996. New catalytic routes for syngas and hydrogen production. *Appl. Catal., A.*, 144, 7–57. DOI: 10.1016/0926-860X(96)00108-1.

Richardson J.T., Paripatayadar S.A., 1990. Carbon dioxide reforming of methane with supported rhodium. *Appl. Catal.*, 61, 293-309. DOI: 10.1016/S0166-9834(00)82152-1.

Rostrup-Nielsen J.R., Sehested J., Norskov J.K., 2002. Hydrogen and synthesis gas by steam- and CO_2 reforming. *Adv. Catal.*, 47, 65–138. DOI: 10.1016/S0360-0564(02)47006-X.

Snoeck J.W., Froment G.F., Fowles M., 2002. Steam/CO_2 reforming of methane. Carbon filament formation by the Boundouard reaction and gasification by CO_2, by H_2 and by steam: Kinetics study. *Ind. Eng. Chem. Res.*, 41, 4252–4265. DOI: 10.1021/ie010666h.

Wang Y.N., Rodrigues A. E., 2005. Hydrogen production from steam methane reforming coupled with in-situ CO_2 capture: Conceptual parametric study. *Fuel*, 84, 1778–1789. DOI: 10.1016/j.fuel.2005.04.005.

Wender I., 1996. Reactions of synthesis gas. *Fuel Process. Technol.*, 48, 189–297. DOI: 10.1016/S0378-3820(96)01048-X.

Xiu G., Li P., Rodrigues A.E., 2003. Adsorption-enhanced steam-methane reforming with intraparticle-diffusion limitations. *Chem. Eng. J.*, 95, 83–93. DOI: 10.1016/S1385-8947(03)00116-5.

York A.P.E., Xiao T., Green M.L.H., 2003. Brief overview of the partial oxidation of methane to synthesis gas. *Top. Catal.*, 22, 345-358. DOI: 10.1023/A:1023552709642.

Zambrano D., Soler J., Herguido J., Menéndez M., 2019. Kinetic study of dry reforming of methane over Ni-Ce/Al_2O_3 catalyst with deactivation. *Top. Catal.*, 62, 456–466. DOI: 10.1007/s11244-019-01157-2.

Zambrano D., Soler J., Herguido J., Menéndez M., 2020. Conventional and improved fluidized bed reactors for dry reforming of methane: Mathematical models. *Chem. Eng. J.,* 393, 124775. DOI: 10.1016/j.cej.2020.124775.

Zhang G., Liu J., Xu Y., Sun Y., 2018. A review of CH_4-CO_2 reforming to synthesis gas over Ni-based catalysts in recent years (2010-2017). *Int. J. Hydrogen Energy*, 43, 15030–15054. DOI: 10.1016/j.ijhydene.2018.06.091.

Received 26 May 2021
Received in revised form 04 August 2021
Accepted 04 August 2021